Neuron, Volume *107*

Supplemental Information

Selective Routing of Spatial Information Flow from Input to Output in Hippocampal Granule Cells

Xiaomin Zhang, Alois Schlögl, and Peter Jonas

Neuron, Volume *107*

Supplemental Information

Selective Routing of Spatial Information Flow from Input to Output in Hippocampal Granule Cells

Xiaomin Zhang, Alois Schlögl, and Peter Jonas

Figure S1, related to Figures 2 and 3. Accurate and efficient detection of individual EPSPs in GCs during spatial navigation

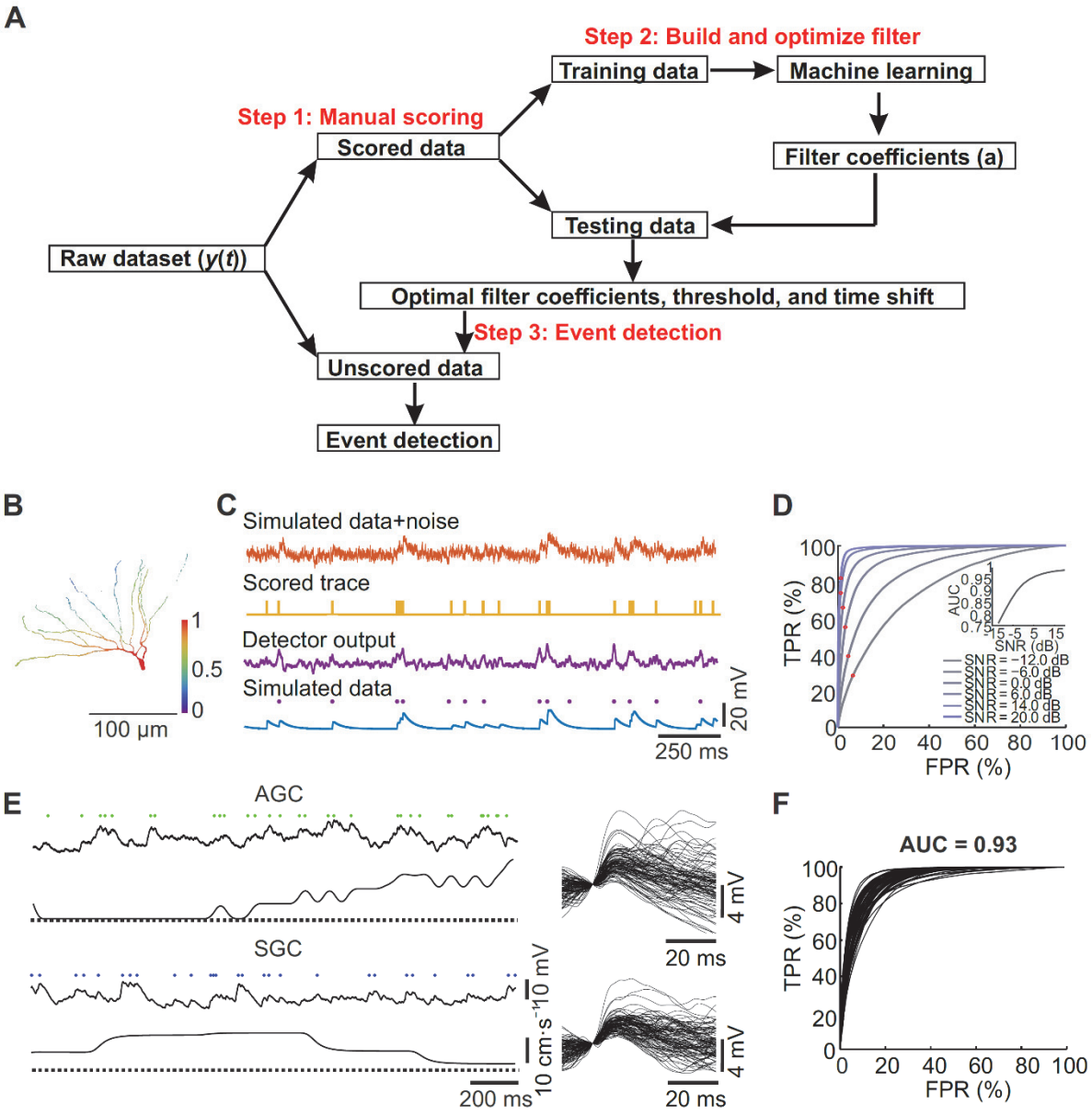

(A) Flowchart of the EPSP detection procedure. After raw data were recorded, parts of the data sets were manually scored by experts. Using these manually scored events, the algorithm was trained to produce an output resembling as closely as possible the manual scoring trace. Optimal filter coefficients were computed based on Wiener-Hopf equation, which was subsequently applied to the original data to generate a raw detection trace.
(B) Generation of synthetic data sets simulating EPSPs in a detailed passive cable model of a GC. Color code indicates normalized somatic EPSP peak amplitude.
(C) Benchmarking the EPSP detection algorithm on synthetic data generated in detailed passive cable model of a GC. Traces show, from top to bottom: (1) simulated data with

added colored noise (signal-to-noise ratio 0 dB), (2) scoring trace generated by applying a symmetric ± 2 ms window to each marker (yellow), (3) raw detection trace generated by the detection algorithm (purple), and (4) underlying simulated data without added noise (blue) overlaid with the detection markers (red).
(D) ROC curves, showing TPR against FPR, for synthetic data with different signal-to-noise ratios (−12, −6, 0, 6, 14, and 20 dB). Red circles, points corresponding to the maximum κ value. Inset, mean AUC, a quantitative measure of detection power and accuracy, plotted versus signal-to-noise ratio.
(E) Subthreshold EPSP activity in an active (top) and a silent (bottom) GC. Top, detection markers; center, EPSP trace; bottom, velocity. Left, continuous traces at compressed time scale; right, individual EPSP traces at expanded scale (vertically aligned to a baseline point preceding the event). In the experiments shown, the AUC was 0.95 for the illustrated active GC and 0.90 for the depicted silent GC.
(F) ROC curve analysis. The mean AUC was 0.93, implying highly reliable detection. Each line represents results from a single GC.

Figure S2, related to Figures 2 and 3. AP rate map and V_m analysis in all active GCs

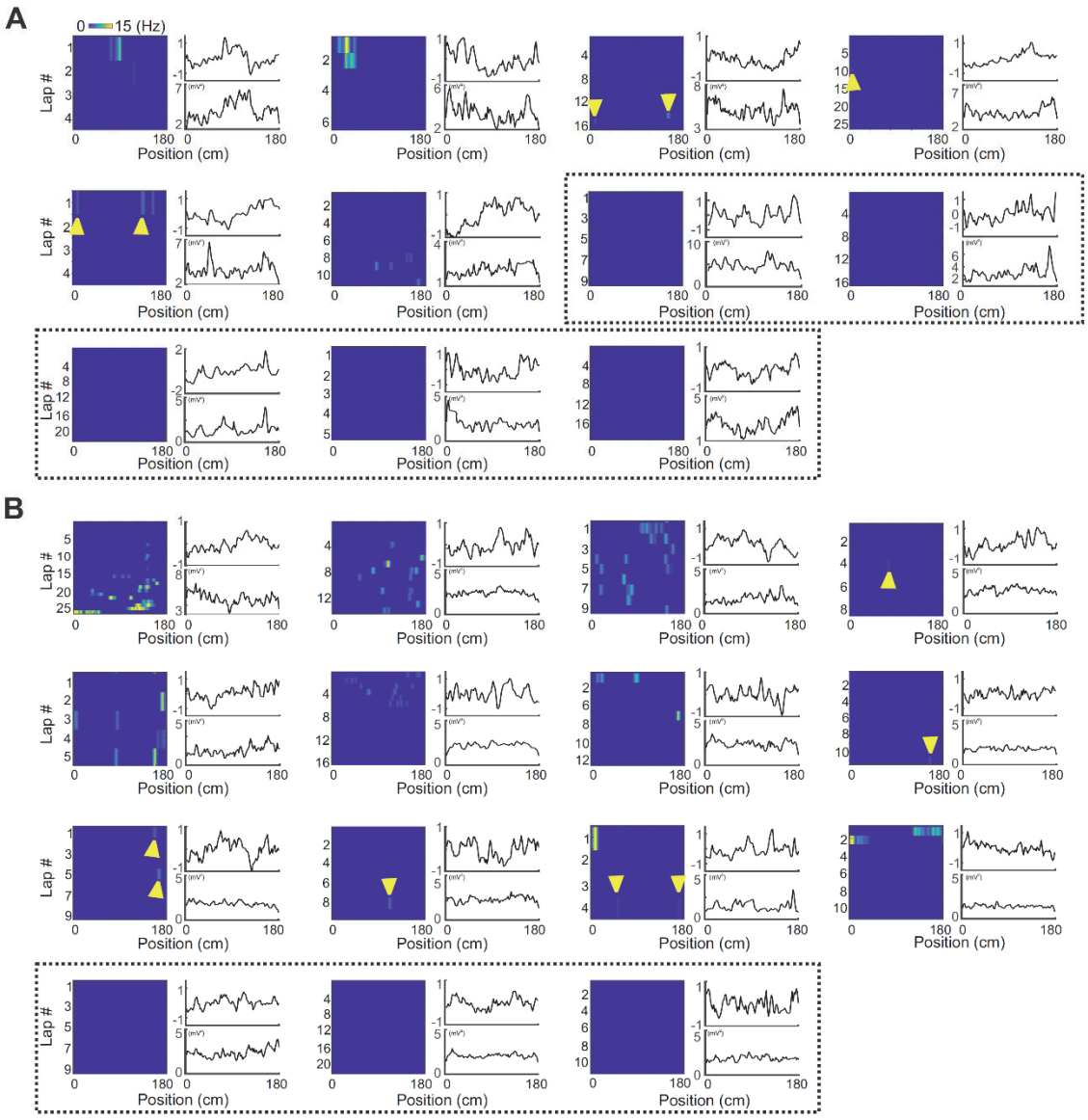

(A) Active GCs in which EPSPs were significantly spatially tuned. Left, AP rate map of a GC. Abscissa represents position on linear belt (2-cm spatial binning), ordinate denotes lap number. Color code scale bar indicates AP frequency in spatial bins (scale bar in upper left panel applies to all panels). Right top, plot of V_m median (after AP removal) against position across laps. Right bottom, plot of V_m variance (after AP removal) against position across laps.

(B) Similar as (A), but for active GCs in which EPSPs were not significantly spatially tuned. In both (A) and (B), yellow arrowheads indicate APs, and dashed black rectangles demarcate cells which were classified as active, but fired APs only during quiet periods; thus, the map was empty.

Figure S3, related to Figures 2–4. Analysis of EPSP frequency, V_m median, and V_m variance as a proxy of synaptic activity confirms spatial tuning of GC input

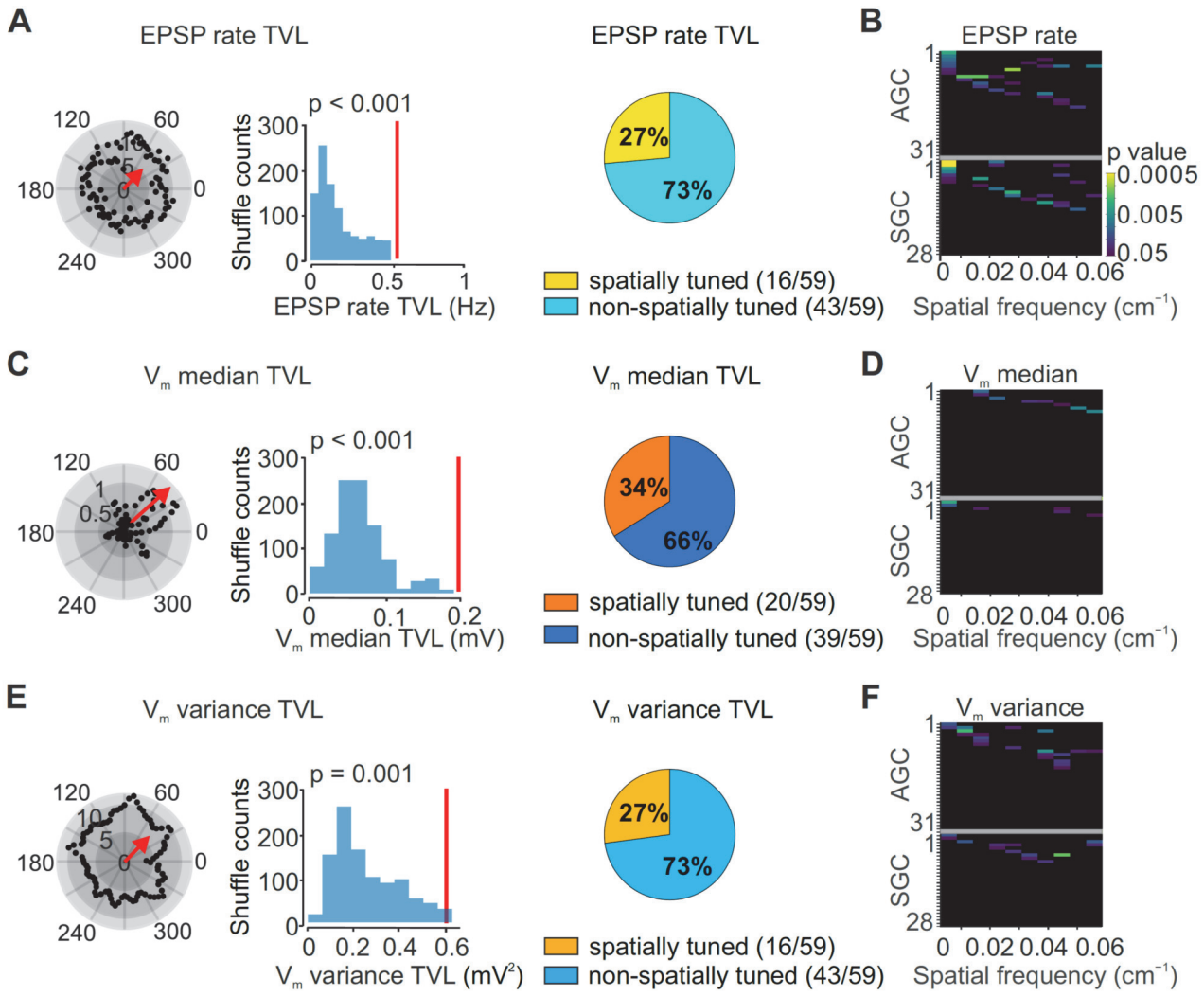

(A) Spatial tuning of EPSP rate with a randomization method in which membrane potential trace and positional trace were shifted by random amounts. Left, polar plot of EPSP event rate. Spatial positions (0–180 cm) were converted into angles (0–360°). Black circles represent EPSP event frequency in each bin (number of events divided by time spent in respective bin). Center, distribution of mean EPSP frequency tuning vector length from randomized data. Red vertical line indicates mean tuning vector length of original data. Note that the mean tuning vector length from the original data is significantly larger than the values obtained from the randomized data. Right, proportion of GCs with spatially tuned synaptic input.

(B) Analysis of statistical significance of Fourier components based on random circular shifting in active (top) and silent (bottom) GCs. Significant differences are shown in color; color code indicates p value. Abscissa shows spatial frequency of the first ten Fourier components, ordinate represents cell index. GCs were sorted according to p values of

individual Fourier components (first according to base component, and then iteratively according to higher-order components).
(C and D) Similar analysis as in (A and B), but for analysis of V_m median.
(E and F) Similar analysis as in (A–D), but for V_m variance. Red arrows in A left, C left, and E left indicate mean tuning vectors (multiplied by 10 for illustration purposes).

Figure S4, related to Figure 4. Minimal place tuning of EPSP peak amplitude in GCs

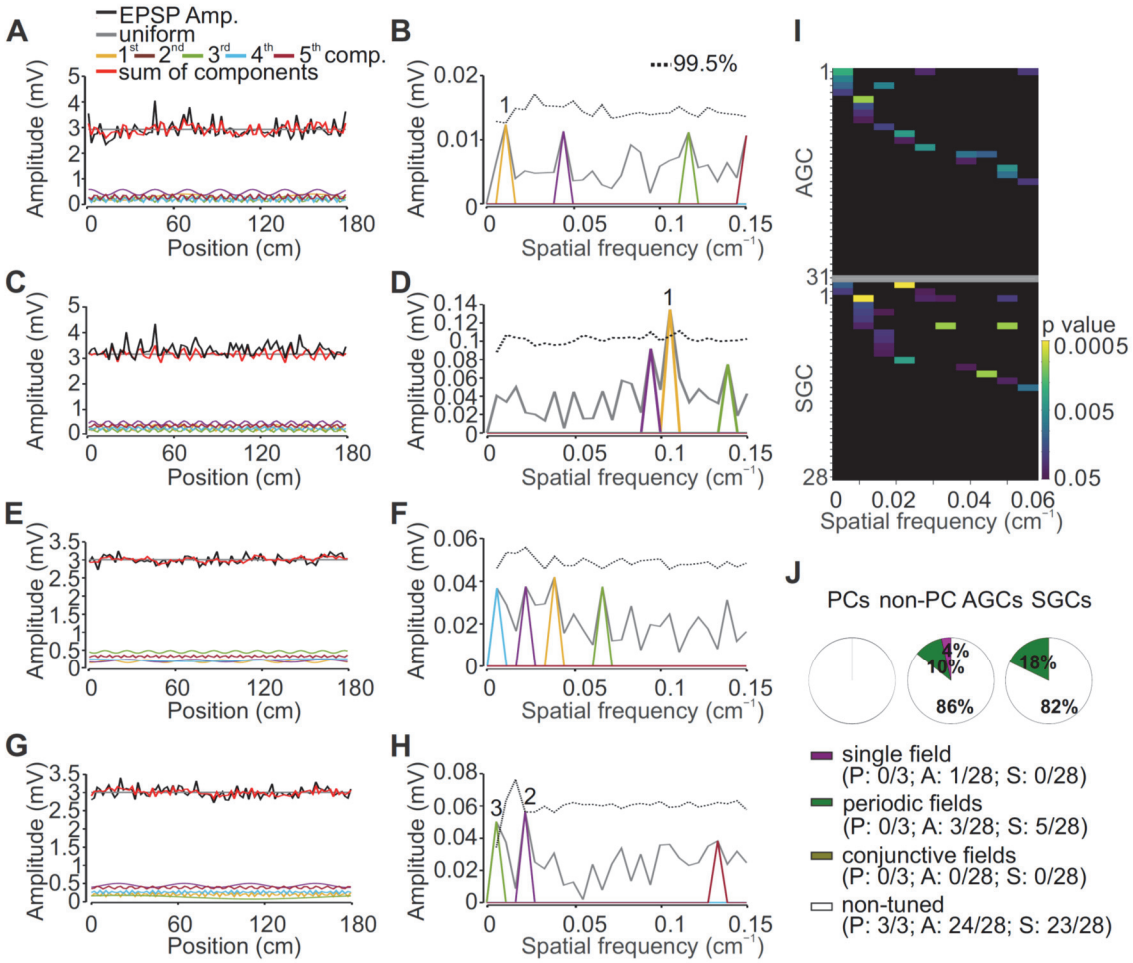

(A–H) EPSP peak amplitude as a function of position in representative GCs (A, C, E, G) and amplitude of spectral components of EPSP amplitude (B, D, F, H). Same cells and representation as shown in Figures 4A–4H. Note that, in contrast to EPSP frequency, EPSP amplitude shows only minimal spatial tuning.

(I) Analysis of statistical significance of Fourier components of EPSP peak amplitude based on shuffling in active (top) and silent (bottom) GCs. Significant differences are shown in color; color code indicates p value (before correction for multiple comparisons). Abscissa shows spatial frequency of the first ten Fourier components, ordinate represents cell index. GCs were sorted according to p values of individual Fourier components (first according to base component, and then iteratively according to higher-order components).

(J) Proportion of active place GC (left), active non-place GCs (center), and silent GCs (right) with single, periodic, and conjunctive field input, based on shuffling ($p < 0.05$; Benjamini-Hochberg correction for multiple comparisons).

Figure S5, related to Figure 5. Place GCs, active non-place GCs, and silent GCs show similar excitatory synaptic input

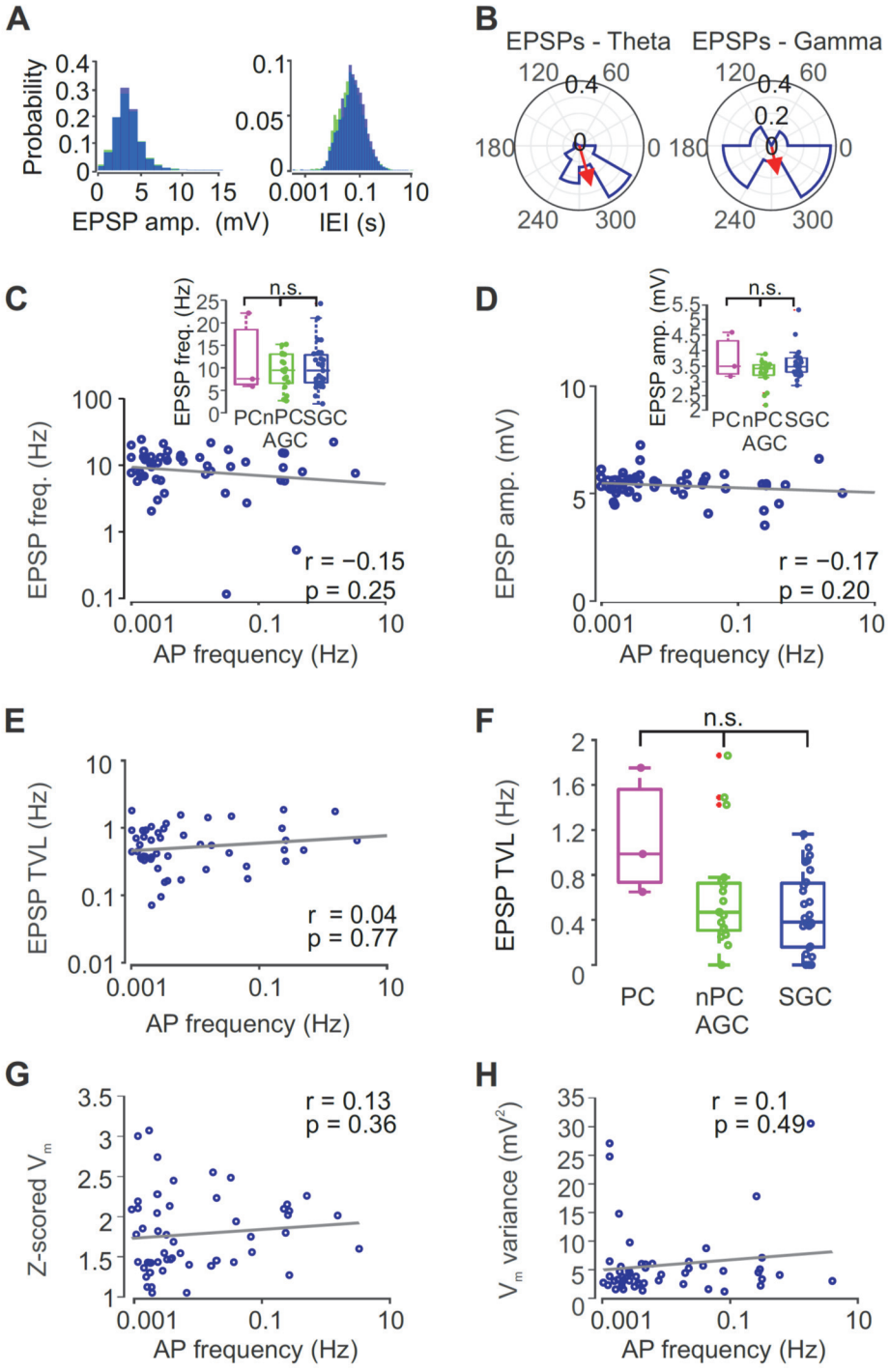

(A) Histogram of EPSP peak amplitudes (left) and EPSP IEIs (right) in active (green) and silent (blue) GCs.

(B) Polar plot of phase preference of EPSPs in relation to theta (left) and gamma (right) oscillations. Red arrow indicates mean tuning vector. Note that EPSPs are significantly phase locked to theta ($p < 0.001$), but not gamma activity ($p = 0.24$), consistent with

previous results (Pernía-Andrade and Jonas, 2014). This confirms the reliability of EPSP detection.
(C and D) Scatter plot of EPSP frequency (C) and EPSP peak amplitude (D), plotted against mean AP frequency (log scale). Inset shows summary bar graph illustrating the parameter for place GCs, active non-place GCs, and silent GCs.
(E and F) Similar plots as shown in (C and D), but for EPSP frequency tuning vector length.
(G and H) Similar scatter plots as shown in (C and D), but for Z-scored V_m and V_m variance. Each data point represents a single GC recording. Lines represent results from linear regression. r, Pearson's correlation coefficient; p, corresponding significance value. None of the parameters is significantly correlated with AP frequency.

Figure S6, related to Figure 3. Properties of spatial information in GCs

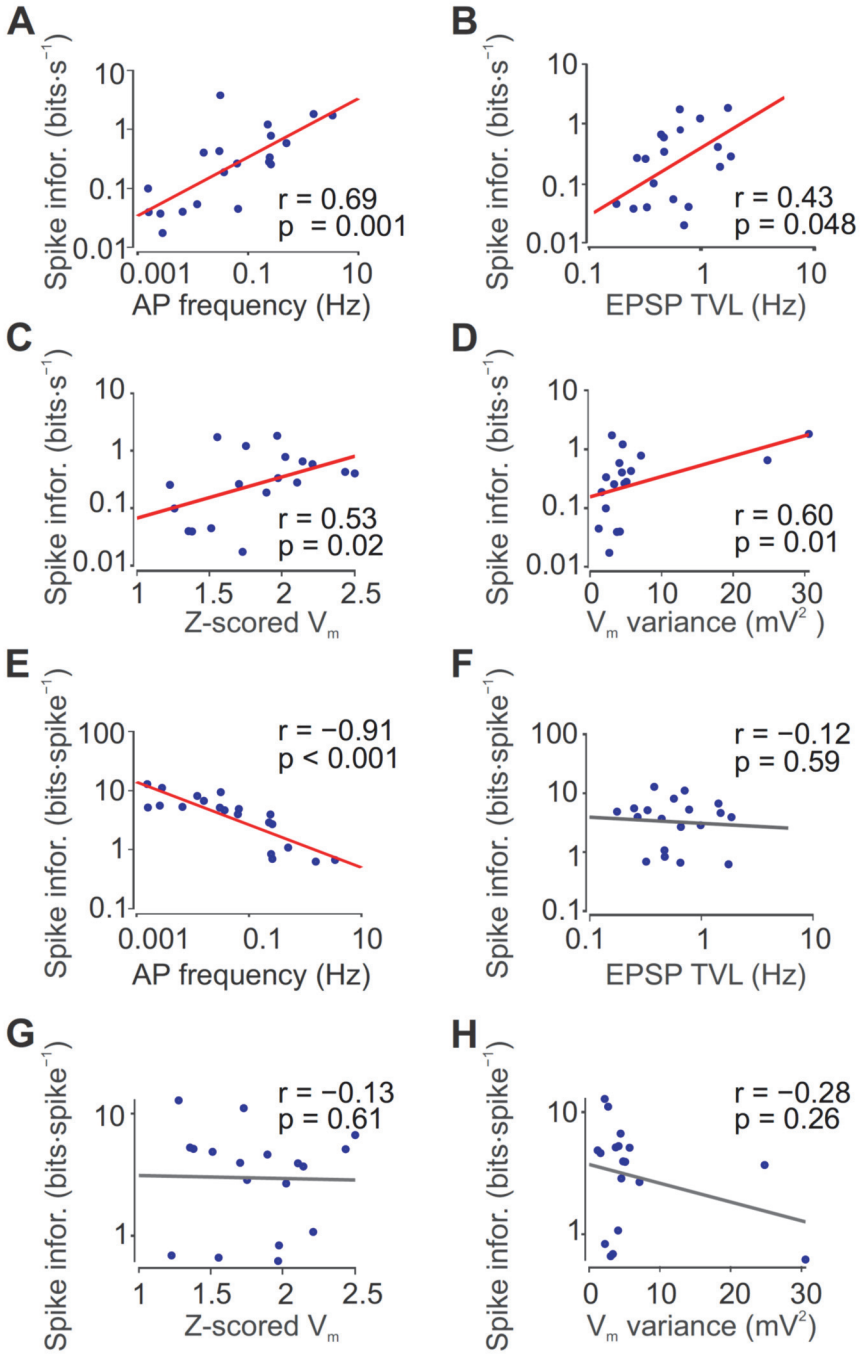

(A–D) Correlation analysis of spatial information given per time, plotted against mean AP frequency (A), EPSP frequency tuning vector length (B, same plot as shown in Figure 3L), Z-scored V_m (C), and V_m variance (D).

(E–H) Similar plots as shown in (A–D), but for spatial information given per spike. Each data point represents a single GC recording. Lines represent results from linear

regression; red line, correlation significant; gray line, correlation not significant. r, Pearson's correlation coefficient; p, corresponding significance value. Note that spatial information per time increases, whereas spatial information per AP decreases as a function of mean AP frequency. Thus, the increase in spatial information is related to an increase in the number of APs. Also note that spatial information per time, but not spatial information per AP is significantly correlated with tuning vector length, Z-scored V_m, and V_m variance. Thus, input-output conversion relies on an increase in the number, rather than the properties of a single spike.

Figure S7, related to Figure 5. Different dendritic architecture, but similar cable properties of active and silent GCs

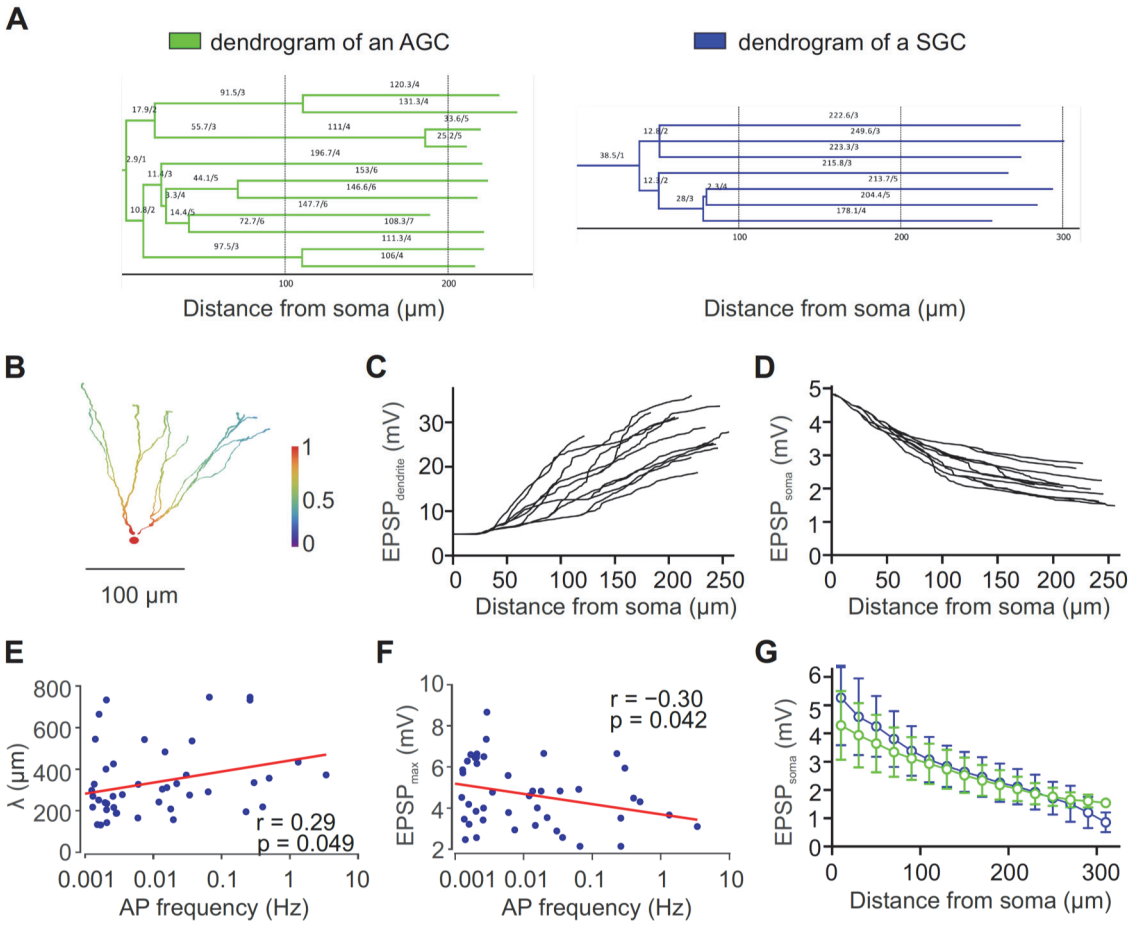

(A) Dendrograms of an active GC (left) and a silent GC (right). Numbers indicate length (in µm) and branch order.
(B) Detailed passive cable model of a reconstructed active GC (mean AP frequency 0.012 Hz). Color code indicates normalized somatic EPSP peak amplitude for synaptic conductances simulated at different dendritic locations.
(C and D) Amplitude of local dendritic (C) and somatic (D) EPSP peak amplitude against distance of synapse from the center of the soma for a reconstructed active GC (same cell as shown in (A, left) and (B).
(E) Plot of length constant λ (decay constant of fit exponential function) against mean AP frequency.
(F) Plot of maximal EPSP peak amplitude at distance = 0 against mean AP frequency.
(G) Comparison of mean somatic EPSP peak amplitude against distance of synapse from the center of the soma for active (green) and silent (blue) GCs. Active cells are slightly less sensitive to proximal inputs in the inner molecular layer, equally sensitive to inputs in the middle molecular layer, and only slightly more sensitive to distal inputs in the outer molecular layer. Thus, cable properties cannot explain the differential activity of GCs.

Figure S8, related to Figures 3–5. Different models of grid-to-place code conversion

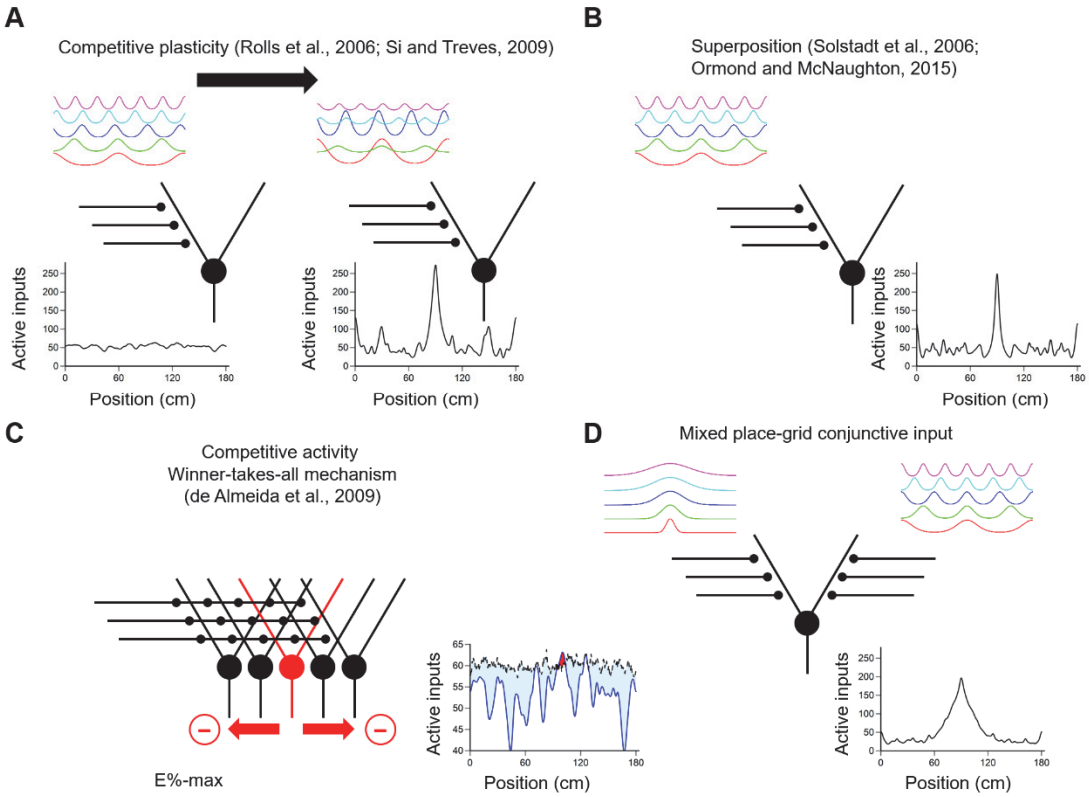

(A) In the “competitive plasticity model”, grid-tuned excitatory GC input becomes place-tuned by Hebbian plasticity (Rolls et al., 2006; Si and Treves, 2009). Curves indicate spatial tuning of input before (left) and after (right) plasticity induction (in the belt center, i.e. at x = 90 cm).
(B) In the “superposition model” or “Fourier model”, place-tuning arises from superposition of grid-tuned inputs with random spatial frequencies, but defined phase (Solstad et al., 2006; Ormond and McNaughton, 2015). Phases of grid-tuned inputs were chosen to give maximal superposition in the belt center, i.e. at x = 90 cm.
(C) In the “network competition model”, individual synaptic inputs are grid-tuned, but the average input is weakly tuned. Place-tuning arises via a competitive network mechanism in which cells with the highest excitation level (red) suppress cells with lower excitation level (black) (de Almeida et al., 2009b). Curves indicate spatial tuning of input in a given cell (blue continuous) and 95% quantile of activity in the total GC population (black dashed). Red area indicates locations in which the activity in the GC exceeds the 95% quantile in the population.
(D) New model in which the GC receives conjunctive input, consistent with the results of the present paper. A fraction of inputs shows place-like tuning (left), whereas another fraction shows grid-like tuning (right). Place fields of place-tuned inputs and phases of grid-tuned inputs were chosen to give maximal superposition in the belt center, i.e. at x = 90 cm.

Table S1, related to Figure 1. Morphological properties of *in vivo* recorded GCs

Morphological parameter	**Active GCs (n = 26)**	**Silent GCs (n = 20)**
Soma location	0.49 ± 0.04 [0 .. 0.85]	0.43 ± 0.04 [0.16 .. 0.71]
Max. branching order	5.85 ± 0.14 [5.. 7]	5.00 ± 0.15 [4 .. 6]
Number of branches at all orders	20.08 ± 0.74 [13.. 29]	18.00 ± 0.83 [12 .. 26]
Number of branches at lower orders (1–3)	7.31 ± 0.38 [4 .. 14]	8.75 ± 0.74 [5 .. 19]
Number of branches at higher orders (4–7)	12.77 ± 0.76 [7.. 24]	9.25 ± 0.93 [2… 16]
Dendritic length at all orders (µm)	1626.7 ± 45.8 [1099.1 .. 2003.8]	1710.3 ± 64.1 [1166.6 .. 2408.3]
Dendritic length at lower orders (1–3) (µm)	382.9 ± 42.6 [91.8 .. 1104.6]	643.2 ± 95.3 [175 .. 1815.8]
Dendritic length at higher orders (4–7) (µm)	1243.8 ± 54.0 [743 ..1668]	1067.1 ± 99.8 [152.3 ... 1855.2]
Convex surface (μm^2)	382.9 ± 42.6 [91.79 .. 1104.6]	643.2 ± 95.2 [174.99.. 1815.8]
Convex volume (μm^3)	1243.8 ± 54.0 [743.04 .. 1668]	1067.1 ± 99.8 [152.29 .. 1855.2]

Values are specified as mean ± SEM [range].

Table S2, related to Figure 5. Passive and active properties of *in vivo* recorded GCs

Functional parameter	**Active GCs (n = 26)**	**Silent GCs (n = 25)**
Resting membrane potential (mV)	−73.0 ± 1.7 [−90.0 .. −54.0]	−73.7 ± 1.5 [−87.8 .. −57.2]
Input resistance (MΩ)	151.8 ± 10.7 [61.0 .. 311.2]	188.1 ± 12.0 [107.4 .. 328.0]
Apparent membrane time constant (ms)	15.1 ± 4.3 [4.5 .. 25.0]	8.5 ± 2.4 [7.8 .. 23.1]
Current threshold (rheobase; in pA)	128.6 ± 13.7 [0 .. 300]	122.0 ± 12.3 [50 .. 250]
Voltage threshold (mV)	−39.4 ± 1.2 [−52.0 .. −26.9]	−35.8 ± 0.9 [−48.1 … −26.6]
AP $(dV / dt)_{max}$	550.1 ± 35.3 [321.1 .. 1003.9]	366.9 ± 27.1 [198.4 .. 729.7]
AP peak amplitude (mV)	77.0 ± 3.1 [52.0 .. 113.8]	62.6 ± 2.5 [38.5 .. 89.3]
AP half-duration (ms)	0.56 ± 0.02 [0.36 .. 0.76]	0.65 ± 0.02 [0.44 ... 0.84]
Max. AP frequency	418 ± 48 [133 .. 1316]	373 ± 30 [159 .. 1000]
Series resistance R_s (MΩ)	47.5 ± 1.7 [26.0 .. 76.3]	50.7 ± 2.1 [34.8 .. 73.6]

Values are specified as mean ± SEM [range].

Table S3, related to Figures 1–5. Total number of GCs and number of GCs used for specific analyses in the present data set

	Active GCs	**Silent GCs**	**Total**	**Reason for exclusion**
Total	39	34	73	
Detailed morphological analysis	26	20	46	Faint labeling or multiple GCs stained
Intrinsic properties	26	25	51	R_s > 80 MΩ; bridge balance suboptimal
AP and EPSP spatial analysis	31	28	59	Mice ran < 4 laps

Table S4, related to Figures 1–5. Action potential activity of GCs and CA1 pyramidal neurons *in vivo* during spatial navigation

	GCs	**CA1 pyramidal neurons**
Total number of cells	73	17
Number of active cells	39	17
Percentage of active cells (%)	53	100
Median AP frequency (Hz)	0.031 ± 0.096	2.56 ± 0.52
Mean, range AP frequency (Hz)	0.125 [0.001, 3]	3.06 [0.004, 10.1]